Search for spatially entangled photon pairs from a 2 mm PPKTP crystal

THESIS

submitted in partial fulfillment of the
requirements for the degree of

BACHELOR OF SCIENCE
in
PHYSICS

Author :	Mila Maxime Schipper
Student ID :	s1173960
Supervisor :	Dr. M.J.A. de Dood
2^{nd} corrector :	Prof.dr. M.A.G.J. Orrit

Leiden, The Netherlands, 31-01-2015

Search for spatially entangled photon pairs from a 2 mm PPKTP crystal

Mila Maxime Schipper

Huygens-Kamerlingh Onnes Laboratory, Leiden University
P.O. Box 9500, 2300 RA Leiden, The Netherlands

31-01-2015

Abstract

In this thesis we study spatially entangled photon pairs created by frequency-degenerate parametric down-conversion from a 2 mm long type-I periodically poled KTP crystal pumped by $\sim$2 ps duration laser pulses. We present measurements of spatial correlations between the entangled photon pairs and compare them to the same measurements performed with a 5 mm PPKTP crystal, shown in [1, paragraph 5.4.2]). For the 5 mm crystal, a peak of coincidences is observed in the collinear direction, which is not in accordance with theoretical predictions. The peak is attributed to quadruplets. We do not observe this extra peak for the 2 mm crystal. Furthermore, we find that the optical alignment is critical and depends on the type of fiber. We conclude that the collection efficiency of the detection units depends on the detection position and decreases away from the collinear direction. Although this observation is not understood, it may contribute to the extra peak. For further research, it is necessary to redesign the detection units to exclude the position dependence of the collection efficiency.

Contents

Chapter 1

Creating entangled photons

When two photons are entangled they share a single quantum mechanical state. As a result the outcome of a measurement on photon 1 is not independent of the measured value for photon 2. At the same time the measurement of a observable of photon 1 is completely random and no information can be extracted. The quantum mechanical description is given by a wave function where the information is shared between both photons.

More precisely, two photons are called entangled if the quantum state of these photons cannot be written as a product state. Let $|\phi\rangle$ and $|\chi\rangle$ be state vectors of photon 1 and 2 respectively and suppose the system of the two photons is in the product state $|\phi \otimes \chi\rangle$. Let A and B be observables of photon 1 and 2 respectively. Suppose their eigenvalue spectra are discrete and denote them by $\{a_n\}$ and $\{b_m\}$. Then the probability $\mathrm{p}(a_n, b_n)$ of observing the eigenvalues a_n and b_m simply equals the product $p_A(a_n)p_B(b_m)$, where $p_A(a_n)$ is the probability of finding eigenvalue a_n when photon 1 is in state $|\phi\rangle$ and $p_B(b_m)$ is the probability of finding eigenvalue b_m when photon 2 is in state $|\chi\rangle$. So if we measure A and B, the outcome of A is independent of that of B.

For an entangled state however, the observables of the individual particles are quantum correlated. A is quantum correlated with B if a measurement of A can change the probability distribution p_B and vice versa. To wit, the measurement of A induces the wave function of the system of two photons to collapse. This collapsed function determines p_B. When A and B are quantum correlated, photon 1 and 2 are said to be entangled in $A\&B$. We shall now discuss a process that can be used to create entangled photons.

1.1 Spontaneous parametric down-conversion

Spontaneous parametric down-conversion (SPDC) is a second order non-linear optical process in which a high-frequency photon splits in two low-frequency photons, which are called the signal and idler photon. The initial photon is called the pump photon. The splitting occurs due to the interaction with a non-linear material. We consider a periodically-poled $KTiOPO_4$ (PPKTP) crystal as the non-linear material, which induces the conversion.

The splitting of the pump photon satisfies the energy conservation law. So the energy of the pump photon equals the combined energy of the signal and idler photon pair:

$$\omega_p = \omega_s + \omega_i \tag{1.1}$$

where ω represents the angular frequency of a photon and p, s and i refers to the pump, signal and idler photon respectively. The signal and idler photon are termed down-converted photons, since their energy is lower than or equal to the energy of the pump photon. We take the propagation direction of the initial photon as the z-direction. Then its wave vector components in the x- and y-direction equal 0. In general we have 'conservation of transverse momentum' (see [2, end of page 4]),

$$(\mathbf{k_s})_x = -(\mathbf{k_i})_x \quad \text{and} \quad (\mathbf{k_s})_y = -(\mathbf{k_i})_y. \tag{1.2}$$

Here $\mathbf{k}$ denotes the wave vector of a photon in the PPKTP crystal. From 1.2 we conclude that the signal and idler photon are anti-correlated in transverse momentum. A phase matching condition, which will be defined in section 1.4, enforces

$$(\mathbf{k_p})_z = (\mathbf{k_s})_z + (\mathbf{k_i})_z.$$

We then have the 'momentum conservation law':

$$\mathbf{k_p} = \mathbf{k_s} + \mathbf{k_i}. \tag{1.3}$$

It follows from equation 1.1 that ω_i and ω_s are equal to

$$\frac{\omega_p \pm \Omega}{2} \tag{1.4}$$

respectively, where Ω is the angular frequency difference of the down-converted photons. In view of equation 1.4 the signal and idler photon are anti-correlated in Ω. We are interested in the frequency-degenerate process, that is

$$\Omega << \omega_p. \tag{1.5}$$

In this case, the signal and idler photons have approximately the same frequency $\omega_p/2$.

The photons are said to be spatially entangled because their positions with respect to the non-linear material are determined by their momenta, classically speaking. The SPDC process is illustrated in figure 1.1.

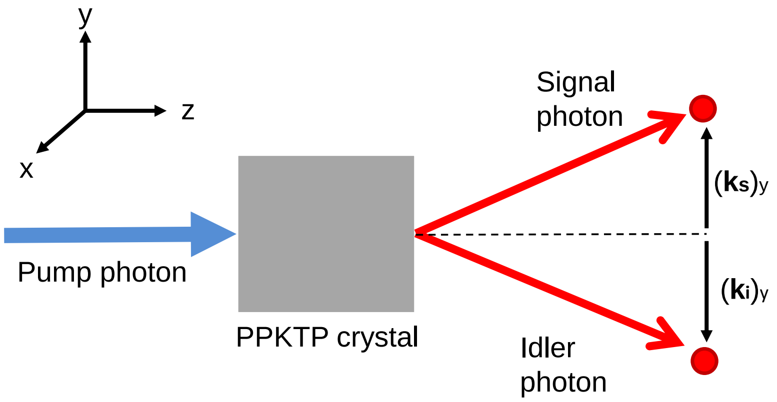

Figure 1.1: *Schematic illustration of the spontaneous parametric down-conversion process. A pump photon propagates in the z-direction and splits into a signal and idler photon due to the interaction with a PPKTP crystal. The* x*- and* y*-components of the signal and idler photon are each other's opposite.*

SPDC is 'spontaneous' because in a classical picture there is no electric field at the frequency of the signal or idler photon to stimulate the process. The process is called 'parametric' because it depends on the initial electromagnetic field, and not only on the intensity of the field. This implies that there exists a relation between the phase of the input and output electromagnetic field.

We consider an SPDC process, where pump, signal and idler photon all have the same polarization. This is accomplished by the use of a type-I PPKTP crystal. We consider plane wave modes represented by $\psi_{\mathbf{k},t}$. $\mathbf{k}$ represents a wave vector and t is associated to a point of time at which the PPKTP crystal is left. Each down-converted photon occupies a linear combination of these modes. For the SPDC light, the plane wave modes are not equal to the Schmidt modes. Therefore there can be uncertainty in both the wave vector $\mathbf{k}$ of a photon and the time t at which it leaves the crystal. We do not need to specify the polarization of an SPDC photon, since this is fixed by the polarization of the pump photon.

Version of 31-01-2015– Created June 24, 2015 - 17:18

1.2 Stimulated parametric down-conversion

At higher pump powers *stimulated* parametric down-conversion gains importance. This is a second order non-linear process in which pump photons are converted into double, triple and in general m-double photon pairs with $m \in \mathbb{N}_{\geq 2}$. The process is called 'stimulated' because an initial photon pair stimulates the creation of an identical pair. By an m-double photon pair we mean m identical pairs of signal and idler photons. So all signal, respectively, idler photons are in the same spatial and temporal mode. In classical terms: They have the same wave vector, frequency, polarisation and they are at the same position at each point in time.

For the PPKTP crystals in this study a process in which the polarisations of all signal and idler photons equal the polarisations of the pump photon is the non-linear process that is phase matched. Hence we omit the polarization in our notation and consider modes of the signal and idler photons that can be represented by $\psi_{\mathbf{k_s},t}$ and $\psi_{\mathbf{k_i},t}$ respectively.

For any signal and idler photon in a m-double photon pair, equation 1.1 and 1.4 hold. We limit the discussion to the frequency-degenerate process, in which 1.5 is valid. If the phase matching conditions are satisfied, equation 1.3 holds for any signal and idler photon. These photons are therefore anti-correlated in transverse momentum. So all signal photons are spatially entangled with all idler photons.

Note that two photon pairs that are in the same temporal mode, do not necessarily form a double pair. The wave vectors of the signal and idler photons need not be the same. This is illustrated in figure 1.2. A similar argument applies to pairs in the same spatial mode that are in different temporal modes. This distinction vanishes if there is only a single spatial and temporal mode.

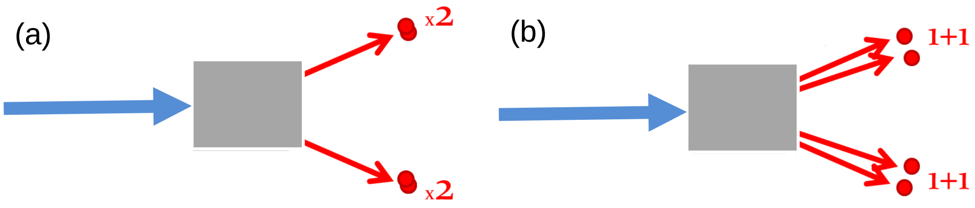

Figure 1.2: *Schematic illustration of photon pairs in the stimulated parametric down-conversion process. In figure (a) a double photon pair is created. In figure (b) two single photon pairs in the same temporal, but in different spatial modes are created.*

At high pump power both spontaneous and stimulated parametric down-conversion occur. This general process is called parametric down-conversion (PDC).

1.3 Laser and filter

A laser is used to create the pump photons in a PDC process. If the power output of the laser is constant over time, it is said to operate in a continuous mode. Otherwise the laser operates in a pulsed mode.

For most continuous-wave lasers used in a PDC experiment, only spontaneous parametric down-conversion occurs. The created single photon pairs are mutually distinguishable in the temporal degree of freedom. This is because the coherence time of most continuous wave lasers, Δt_{laser} is much longer than the coherence time of the PDC light, Δt_{PDC}. To wit, the number of points of time that can be distinguished, N, equals

$$N = \sqrt{1 + \left(\frac{\Delta t_{laser}}{\Delta t_{PDC}}\right)^2}. \tag{1.6}$$

(See [equation (2) and (9)][7].) So if $\Delta t_{laser} \gg \Delta t_{PDC}$, N is very large and all points in time at which a photon pair is created, can be distinguished.

If a pulsed laser is used, stimulated parametric down-conversion occurs as well as spontaneous parametric down-conversion since the instantaneous laser power increases. Furthermore, the coherence time of a pulsed laser is smaller than the coherence time of a continuous wave laser. Consequently less points in time can be distinguished. We conclude that the points in time at which (m-double) photon pairs are created, can in general not be distinguished. This causes the (m-double) photon pairs to be indistinguishable in the temporal degree of freedom. Note that the (m-double) photon pairs can still be distinguishable in the spatial degree of freedom. In our experiment we use a laser that operates in a pulsed mode.

As is mentioned above, we are interested in frequency degenerate parametric down-conversion. In order to measure only (m-double) photon pairs that satisfy equation 1.5, we filter out the other pairs. In our experiment, we use a bandpass filter centered around $\omega_p/2$. This filter also serves to spectrally filter the PDC light to increase the coherence time to operate in a regime with a few temporal modes.

1.4 Far field intensity distribution of PDC light

We regard a laser pumping a type-1 PPKTP crystal. Furthermore, we consider the created PDC light to be filtered by a bandpass filter, centered around $\omega_p/2$. The propagation direction of the pump photons is taken as the z-direction.

Let $\mathbf{k_s}$ and $\mathbf{k_i}$ be the wave vectors of a signal and idler photon in an (m-double) photon pair. Because of the frequency-degeneracy, we have

$$|\mathbf{k_s}| = \frac{\omega_p/2 \cdot n(\omega_p/2)}{c} = |\mathbf{k_i}| =: k_d. \tag{1.7}$$

In this equation n denotes the temperature and frequency dependent refractive index of the crystal. In principle n is direction-dependent. By 1.2 and since we consider type-I down-conversion, n is equal for the propagation direction of the signal and idler photon. k_d refers to the wave number of the down-converted photons. From 1.7 and 1.2 it follows that $(\mathbf{k_s})_z$ and $(\mathbf{k_i})_z$ are equal in amplitude. In our case the signal and idler photons travel in the same direction, that is

$$(\mathbf{k_s})_z = (\mathbf{k_i})_z =: k_{d,z}. \tag{1.8}$$

The far-field of the source is created in the focal plane of a lens that is placed a focal distance behind the crystal. We can measure the intensity distribution of PDC light in the far field with a CCD camera. Each position (x^*, y^*) in this far field plane corresponds to a certain transverse momentum (q_x, q_y) of a down-converted photon. To wit, a down-converted photon with this momentum produced at the center of the crystal would arrive at the position (x^*, y^*) in the far field, classically speaking. So the PDC intensity distribution I can be represented as a function of q_x and q_y. By symmetry around the z-axis, the intensity only depends on $q = \sqrt{q_x^2 + q_y^2}$. We have

$$I(q, T) \propto \operatorname{sinc}^2\left(\frac{L}{2k_d}q^2 + \phi(T)\right). \tag{1.9}$$

This is derived from [1, equation 2.3] by setting $\sigma = 0$. Namely, we then integrate over a delta function centered around $\Omega = 0$. In 1.9 the length of the non-linear material in the z-direction is represented by L and ϕ is the phase mismatch defined by

$$\phi(T) := \frac{1}{2}L\Delta k(T).$$

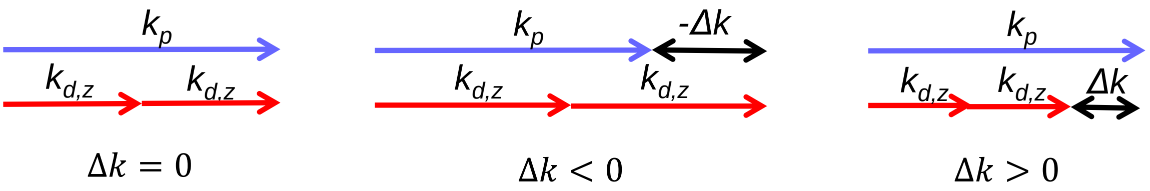

Figure 1.3: *Schematic illustration of k_p and $k_{d,z}$ for wave vector mismatches $\Delta k = 0$, $\Delta k < 0$ and $\Delta k > 0$.*

In this equation

$$\Delta k := k_p - (\mathbf{k_i})_z - (\mathbf{k_s})_z$$

denotes the wave vector mismatch with $k_p := |\mathbf{k_p}| = (\mathbf{k_p})_z$, the wave number of the pump photon. By equation 1.8, we have

$$\Delta k(T) = k_p - 2k_{d,z} \approx k_p - 2k_d. \tag{1.10}$$

If we neglect the contribution of the transverse components to k_d, as in 1.10, we can give the following simple expressions for the wave vector mismatch:

$$\Delta k(T) \approx \frac{\omega_p}{c}(n(\omega_p, T) - n(\omega_p/2, T)),$$

where n is the refractive index of the PPKTP crystal. Note that we also neglect the fact that n is direction dependent. (This effect is small since $k_{d,z} \approx k_z$.) We conclude that the phase mismatch and therefore the intensity distribution are temperature dependent. We will now see *how* the intensity depends on T.

From equation 1.9 it follows that the intensity distribution is at its maximum for a value of q that satisfies

$$\frac{L}{2k_d}q^2 + \phi(T) = 0. \tag{1.11}$$

Away from this particular q the intensity decreases rapidly. Δk and therefore ϕ can be 0, negative or positive, depending on the crystal temperature. See figure 1.3.

The condition $\phi = 0$ is called the phase matching condition. It occurs only for a specific crystal temperature and we refer to this process as collinear down-conversion. From 1.11 we conclude that the intensity is at its maximum for $q = 0$ if the phase matching condition is satisfied. Therefore the intensity distribution forms a disk centered around $q = 0$. This is shown in figure 1.4(a). (Note that x and y refer to q_x and q_y respectively.) If $\phi < 0$, the intensity reaches its maximum for

$$q^* = \frac{-2k_d\phi}{L}.$$

In this case the intensity distribution forms a ring with radius q^*, which is shown in figure 1.4(b). If $\phi > 0$, equation 1.11, can't be satisfied since the first term is positive. In this case, the intensity distribution forms a weak spot centered around $q = 0$. If the phase-matching condition is not satisfied, we speak of non-collinear PDC light.

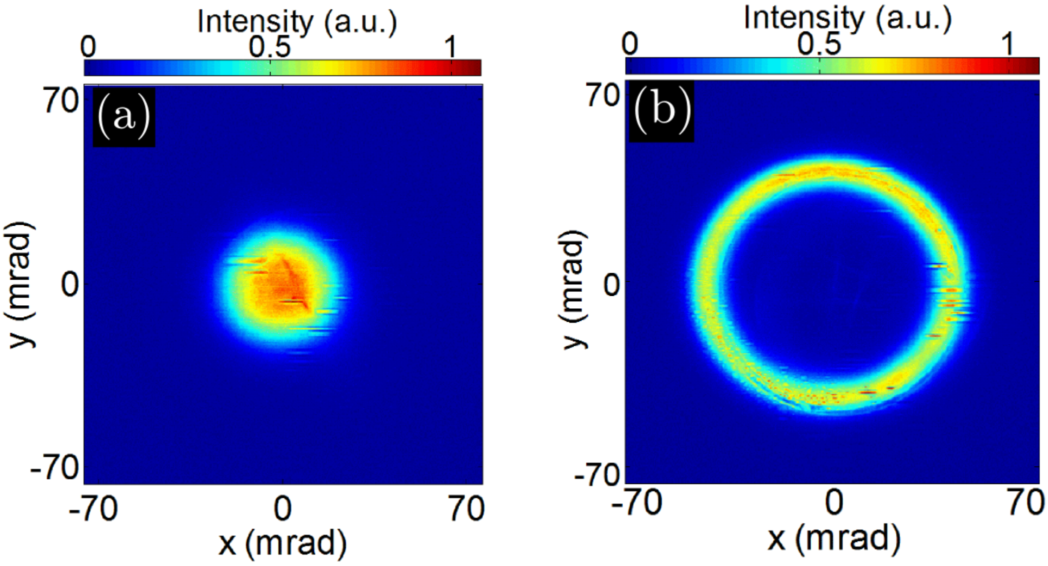

Figure 1.4: *CCD images of the PDC intensity distribution in the far field for two crystal temperatures T. A laser produces 2 ps long pulses at 413.2 nm and pumps a 2 mm PPKTP crystal. The created PDC light is filtered by a 1 nm FWHM band-pass filter. The image is taken from [1, figure 2.3]. (a) $T = 50°C$, (b) $T = 30°C$. In figure (a) the intensity distribution is disk shaped. The phase matching conditions are approximately satisfied, so we speak of collinear PDC light. In figure (b) non-collinear down-conversion occurs, since the intensity distribution is ring-shaped. In this figure x and y correspond to q_x and q_y in the text.*

As a matter of fact, equation 1.9 is only valid for a continuous-wave laser. A pulsed laser has a non-zero spectral width. The intensity-distribution of the pump as a function of the angular frequency, $I_p(\Omega)$, is Gaussian with a standard deviation σ, i.e. it can be written as

$$I_p(\Omega) = \frac{1}{\sigma\sqrt{2\pi}} \exp\left(-\frac{1}{2}((\Omega - \omega_p)/\sigma)^2 \right).$$

The non-zero spectral width causes the sinc function of 1.9 to spread out. Furthermore the different frequency components within the laser pulse lead to a slightly different phase matching condition, defined by

$$\phi(T) + \frac{1}{2} D\Omega L = 0.$$

Here D is the dispersion defined by $D = (n_g(\omega_p) - n_g(\omega_p/2))/c$, with n_g is the group index of the crystal. The intensity distribution can be written as

$$I(q,T) \propto \int_{-\infty}^{\infty} d\Omega \exp\left(-\frac{1}{2}(\Omega/\sigma)^2\right) \times \operatorname{sinc}^2\left(\frac{L}{2k_d}q^2 + \phi(T) + \frac{1}{2}D\Omega L\right). \tag{1.12}$$

where σ is the standard deviation of the intensity distribution as a function of the angular frequency of the pump. (See [1, equation 2.3].)

Chapter 2

State reached by parametric down-conversion

2.1 Light

The physicist James Clerk Maxwell has shown that the electric and magnetic field can form a wave, propagating at the speed of light. Since then, light is described as an electromagnetic wave. In the classical description, the electromagnetic field consists of an electric field $\mathbf{E}(\mathbf{r}, t)$ and a magnetic field $\mathbf{B}(\mathbf{r}, t)$, which satisfy Maxwell's equations. Each light wave can be expressed as a linear combination of monochromatic plane waves. These plane waves are fully characterised by a wave vector $\mathbf{k}$, a polarisation s, a phase ϕ and an amplitude A.

In quantum optics the electromagnetic field is quantised, i.e. the electromagnetic field is described quantum-mechanically and its total energy has only discrete values. The electric and magnetic field are described by operators acting on a certain complex vector space. This vector space has an orthonormal basis of photon number eigenstates

$$\{|(n_{\mathbf{k},s})_{\mathbf{k}\in\mathbb{R}^3,\ s\in\{0,\frac{\pi}{2}\}}\rangle : n_{\mathbf{k},s} \in \mathbb{N} \text{ for all } \mathbf{k} \text{ and } s\}. \tag{2.1}$$

The eigenstate $|(n_{\mathbf{k},s})_{\mathbf{k}\in\mathbb{R}^3,\ s\in\{0,\frac{\pi}{2}\}}\rangle$ is referred to as a state with $n_{\mathbf{k},s}$ 'photons' with wave vector $\mathbf{k}$ and polarisation s. The state with zero photons for each wave vector and polarisation, $|(0)_{\mathbf{k}\in\mathbb{R}^3,\ s\in\{0,\frac{\pi}{2}\}}\rangle$, is called the vacuum state. A state with $n_{\mathbf{k},s}$ photons with wave vector $\mathbf{k}$ and polarisation s and 0 photons for the other wave vectors and polarisations is also denoted simply by $|n_{\mathbf{k},s}\rangle$.

In analogy to the classical description in the first paragraph, quantised light can be described as a normalised linear combination of photon number eigenstates. These states are characterised by a wave vectors $\mathbf{k}$, polarisations s and number of photons n.

It is useful to introduce a creation and annihilation operator for each wave vector $\mathbf{k}$ and polarisation s, denoted by $a^{\dagger}_{\mathbf{k},s}$ and $a_{\mathbf{k},s}$ respectively. The photon number states form a basis of eigenvalues for both operators with

$$a^{\dagger}_{\mathbf{k},s}|(n_{\mathbf{k}',s'})_{\mathbf{k}',s'}\rangle = |(n'_{\mathbf{k}',s'})_{\mathbf{k}',s'}\rangle$$

with

$$n'_{\mathbf{k}',s'} = \begin{cases} n_{\mathbf{k}',s'} & \text{if } (\mathbf{k}',s') \neq (\mathbf{k},s). \\ \sqrt{n_{\mathbf{k},s}+1}(n_{\mathbf{k},s}+1) & \text{if } (\mathbf{k}',s') = (\mathbf{k},s). \end{cases} \tag{2.2}$$

Therefore $a^{\dagger}_{\mathbf{k},s}$ is said to create a photon with wave vector $\mathbf{k}$ and polarisation s. An equation similar to 2.2 can be given for the annihilation operator. Not surprisingly, this operator annihilates a photon with corresponding wave vector and momentum. The following elegant expressions can be given for the creation, respectively annihilation operators:

$$a^{\dagger}_{\mathbf{k},s} = \sum_{n=0}^{\infty} \sqrt{n+1}|(n+1)_{\mathbf{k},s}\rangle\langle n_{\mathbf{k},s}|, \tag{2.3}$$

$$a_{\mathbf{k},s} = \sum_{n=0}^{\infty} \sqrt{n+1}|n_{\mathbf{k},s}\rangle\langle (n+1)_{\mathbf{k},s}|. \tag{2.4}$$

The creation and annihilation operators satisfy the following commutation relations:

$$[a_{\mathbf{k},s}, a^{\dagger}_{\mathbf{k}',s'}] = \delta_{\mathbf{k},\mathbf{k}'}\delta_{s,s'}I. \tag{2.5}$$

In paragraph 2.3 we will see that this mathematical property is very useful in the theoretical description of PDC. We will first focus on the mathematics of operator ordering theorems, of which one is needed in paragraph 2.3.

2.2 Operator ordering theorems

The exponential function is of great importance in quantum mechanics. If the state of a quantum system $|\psi\rangle$ is given at an initial time ($t = 0$) and if the Hamiltonian H is independent of time, we can compute the quantum state at any subsequent time by

$$|\psi(t)\rangle = \exp(-iHt/\bar{h})|\psi(0)\rangle. \tag{2.6}$$

For any operator A, its exponent $\exp(A)$, is defined by the usual power series expansion

$$\exp(A) = \sum_{n=0}^{\infty} \frac{A^n}{n!}. \tag{2.7}$$

The operator $\exp(-iHt/\bar{h})$ is named the time-evolution operator. This operator can often be represented as the sum of certain operators A and B

$$-iHt/\bar{h} = A + B. \tag{2.8}$$

In this case it is useful to 'order' the time evolution operator so as to compute the right-hand side of equation 2.6. By ordering we mean rewriting the time evolution operator as a product of exponential factors, including $\exp(\lambda A)$ and $\exp(\lambda' B)$ for certain $\lambda, \lambda' \in \mathbb{C}$. The form of the ordering is related to the commutation relations for the operators involved. For two operators A and B we define the commutator $[A, B] := AB - BA$. For example if $[A, B] = 0$, that is A and B commute, we have a simple ordering:

$$\exp(A + B) = \exp(A) \exp(B). \tag{2.9}$$

If A and B both commute with their commutator, i.e.

$$[A, [A, B]] = [B, [A, B]] = 0,$$

we have a more complicated ordering:

$$\exp(A + B) = \exp(A) \exp(B) \exp\Big(-\frac{1}{2}[A, B]\Big). \tag{2.10}$$

These are examples of so called operator ordering theorems.

More general $\exp(A) \exp(B) = \exp(C)$ with

$$C = A + B + \frac{1}{2}[A, B] + \frac{1}{12}([A, [A, B]] - [B, [A, B]]) + \text{ higher-order terms }. \tag{2.11}$$

According to the Campbell-Hausdorff theorem, C is a series in which all terms are linear combinations of iterated commutators in A and B. (See [5].) In quantum mechanics, we can often choose an order high enough such that all nested commutators of this order equal 0. It then follows that all higher-order nested commutators are 0 as well. The operator C in formula 2.11 can be expressed as a finite sum and an operator ordering theorem can be derived. For example, the orderings 2.9 and 2.10 are both implied by the Campbell-Hausdorff theorem. (See appendix 7.1.)

To give a theoretical description of parametric down-conversion, we need another ordering theorem, which we shall present now. For operators K_+, K_- and K_3, satisfying

$$[K_3, K_\pm] = \pm K_\pm, \tag{2.12a}$$
$$[K_+, K_-] = -2K_3, \tag{2.12b}$$

and complex numbers γ_+ and γ_-, we have the following lengthy ordering

$$\begin{aligned}\exp(\gamma_+ K_+ + \gamma_- K_-) &= \exp\Big(-i\sqrt{\frac{\gamma_+}{\gamma_-}}\tanh(\beta)K_+\Big) \\ &\times \exp(-2\ln(\cosh(\beta))K_3)\exp\Big(-i\sqrt{\frac{\gamma_-}{\gamma_+}}\tanh(\beta)K_-\Big), \\ &\text{with } \beta = i\sqrt{\gamma_+\gamma_-}\end{aligned} \tag{2.13}$$

Equation 2.13 can in principle be derived from the Campbell-Hausdorff formula. However, since equation 2.11 does not become a finite sum for any (non-trivially chosen) operators A and B in this situation, this is a tedious job. An simpler way to prove equation 2.13 is shown in [4, pages 42-46].

2.3 Theoretical description of PDC

We will now give a theoretical description of parametric down-conversion. In order to do this we will exploit the commutation relation 2.5 and operator ordering theorem 2.13. If an electromagnetic field propagates in a strong, undepleted, coherent state $|\gamma\exp(-i\omega_P t)\rangle$ through a material with non-linear susceptibility $\chi^{(2)}$, down-converted photons at frequency ω_s and ω_i can be created. In the parametric approximation the creation and annihilation operator for the pump can be replaced by $\gamma^*\exp(i\omega_p t)$ and $\gamma\exp(-i\omega_p t)$. The interaction Hamiltonian for this process is given by

$$H_{int} = i\hbar(\kappa^* a_s^\dagger a_i^\dagger - \kappa a_s a_i) \tag{2.14}$$

with $\kappa := \chi^{(2)}_{z,z,z}\gamma$, where $|\gamma|^2$ equals the mean photon number. (See [3, pages 182-187].) Here $\chi^{(2)}_{z,z,z}$ is the (z,z,z)-component of the 3-tensor $\chi^{(2)}$ and κ^* denotes the complex conjugated of κ. The resonant frequency of the PPKTP crystal is far away from the pump frequency, so we operate in a non-resonant regime, which causes $\chi^{(2)}_{z,z,z}$ to be real. Since γ is real, so is κ are real, i.e. $\kappa = \kappa^*$. Furthermore $a_s^\dagger$ and $a_i^\dagger$ are the creation operators for the signal and idler photons. a_s and a_i denote the annihilation operators. We let the time-evolution operator of the Hamiltonian act on the vacuum state to find the created quantum states. So we calculate

$$\exp(-iH_{int}t/\hbar)|0\rangle = \exp(\kappa t(a_s^\dagger a_i^\dagger - a_s a_i))|0\rangle, \tag{2.15}$$

where t is the time it takes the pump beam to travel through the PPKTP crystal. (Since the refractive index of the crystal is lower for the PDC frequency compared to the pump frequency, equation 2.15 is only an approximation of the created quantum states.) In order to compute the right hand side of equation 2.15 we need to disentangle the exponent. This is where an operator ordering theorem is required.

We first consider the case where the signal and idler photon are not in the same spatial mode (their transverse momenta are non-zero), such that

$$a_s^\dagger \neq a_i^\dagger \text{ and} \tag{2.16a}$$
$$a_s \neq a_i. \tag{2.16b}$$

This is referred to as the non-collinear geometry, which should be distinguished from non-collinear *down-conversion*. Let q be the amplitude of the transverse momenta of the signal and idler photon. We shall denote the created quantum state by $|\psi_q\rangle$. Define

$$K_+ := a_s^\dagger a_i^\dagger, \tag{2.17a}$$
$$K_- := a_s a_i, \text{ and} \tag{2.17b}$$
$$K_3 := \frac{1}{2}(a_s^\dagger a_s + a_i a_i^\dagger) \tag{2.17c}$$

One can verify that the commutation relations 2.12 are satisfied. For example we have

$$\begin{aligned}[K_+, K_-] &= [a_s^\dagger a_i^\dagger, a_s a_i] \\ &= a_s^\dagger a_s [a_i^\dagger, a_i] + a_s^\dagger [a_i^\dagger, a_s] a_i + a_s [a_s^\dagger, a_i] a_i^\dagger + [a_s^\dagger, a_s] a_i a_i^\dagger \\ &= -(a_s^\dagger a_s + a_i a_i^\dagger) \\ &= -2K_3\end{aligned}$$

In the last equality we have used the commutation relation 2.5. Note that $a_s^\dagger$ and a_s commute with a_i and $a_i^\dagger$ respectively since i, s denote different spatial modes. Now, we invoke our ordering 2.13 to obtain the disentangled expression

$$\begin{aligned}&\exp(\kappa t(a_s^\dagger a_i^\dagger - a_s a_i)) = \exp\Big(\tanh(|\kappa|t) a_s^\dagger a_i^\dagger\Big)\\ &\times \exp(-\ln(\cosh(|\kappa|t))(a_s^\dagger a_s + a_i a_i^\dagger))\exp\Big(\tanh(|\kappa|t) a_s a_i\Big).\end{aligned} \tag{2.18}$$

This expression is lengthy, but very useful. Because the quantum states that are created by parametric down-conversion can be found, by letting 2.18 act on the vacuum state. We let each of the three exponents act step by step, which is shown in appendix 7.2. It follows that

$$|\psi_q\rangle = \sum_{j=0}^{\infty} \frac{\tanh(|\kappa|t)^j}{\cosh(|\kappa|t)} |j_q, j_{-q}\rangle, \tag{2.19}$$

where $|j_q, j_{-q}\rangle$ is a state with j signal and j idler photons. So $|\psi_q\rangle$ is a superposition of single and j-multiple photon states.

Now, we consider the case where the signal and idler photon are in the same spatial mode. This is called the collinear geometry, which should not be mixed up with collinear *down-conversion*. Let $a_0^\dagger$ and a_0 denote the creation, respectively annihilation operator of both the signal and idler photon. We will refer to the created quantum state as $|\psi_0\rangle$. We define the operators

$$K_+ := \frac{1}{2}(a^\dagger)^2, \tag{2.20a}$$

$$K_- := \frac{1}{2}a^2, \text{ and} \tag{2.20b}$$

$$K_3 := \frac{1}{4}(a^\dagger a + a a^\dagger), \tag{2.20c}$$

which satisfy the commutation relations in 2.12. Analogously to the derivation above, it can be shown that

$$|\psi_0\rangle = \sum_{j=0}^{\infty} \frac{\sqrt{(2j)!}}{j!} \Big(\frac{1}{2}\Big)^j \frac{\tanh(|\kappa|t)^j}{\sqrt{\cosh(|\kappa|t)}} |2j_0\rangle. \tag{2.21}$$

The state $|2j_0\rangle$ refers to a state with 2 down-converted photons with transverse momentum equal to 0. Note that $|\psi_0\rangle$ is a superposition of only even-numbered photon states.

One can show that the state vectors in 2.19 and 2.21 are normalised wave functions. Since $\tanh(|\kappa|t) < 1$, the probability to measure a j-double photon pair decreases with j. Furthermore, if the amplitude of

(z, z, z)-component of the non-linear suscepitibility, $|\chi^{(2)}_{z,z,z}|$, or the strength of the pump power γ increases, so does $|\kappa|$. The time t is proportional to the length of the crystal an can thus be increased. In our experiment $|\kappa|t \ll 1$. Therefore the states 2.19 and 2.21 can be approximated by Taylor expansions around $|\kappa|t = 0$. (See [1, page 73].) This gives

$$|\psi_q\rangle \approx (1 - \frac{(|\kappa|t)^2}{2})|0\rangle + |\kappa|t|1_q; 1_{-q}\rangle + (|\kappa|t)^2|2_q; 2_{-q}\rangle, \tag{2.22a}$$

$$|\psi_0\rangle \approx (1 - \frac{(|\kappa|t)^2}{4})|0\rangle + \frac{1}{\sqrt{2}}|\kappa|t|2_0\rangle + \sqrt{\frac{3}{8}}(|\kappa|t)^2|4_0\rangle. \tag{2.22b}$$

The probability to create a photon pair, instead of the vacuum state, increases if $|\kappa|t$ does. This increase goes with $(|\kappa|t)^j$ for a j-double photon pair. We conclude that the probability to find a j-double photon pair compared to a $(j-1)$-double pair increases if $|\kappa|t$ does, for all $j \in \mathbb{N}_{\geq 1}$.

Version of 31-01-2015– Created June 24, 2015 - 17:18

Chapter 3

Experimental apparatus

3.1 Setup

In this section we describe our experimental setup, which is depicted in figure 3.1. This setup measures correlations between the momentum of photon pairs by detecting coincidences between detectors D_A and D_B. The beamsplitter BS allows to also look at photons emitted in the same direction.

The photon pairs are generated in the crystal (C) pumped by a pulsed titanium-sapphire lasers that produces 2 ps long pulses at 826.4 nm. This laser operates at a repetition rate of 80 MHz. Pulses at 413.2 nm are created by a process called second harmonic generation. The created laser beam is called the pump beam. A blue filter RB blocks the red light, that is not converted into blue light. A lens L_1 with a focal length of 150 mm is used to focus the pump beam at a type-I, 2 mm long, periodically-poled $KTiOPO_4$ (PPKTP) crystal C. The PDC process converts the 413.2 nm pump light in red down-converted light. The angular frequencies of the signal and idler can satisfy equation 1.1 in many ways. Therefore, the PDC light consists of different frequencies. The wavelengths of the PDC light are symmetrically distributed around 826.4 nm. Since the pump laser is pulsed, stimulated parametric down-conversion occurs besides spontaneous parametric down-conversion.

The temperature of the crystal is set by a temperature controller TC. A long-pass filter blocks all light below 720 nm, which includes the blue pump light. A gallium phosphide wafer, GaP, anti-reflection coated for wavelengths centered around $\sim$826 nm, is used to fully block the 413.2 nm pump light. We collect the down-converted photons in the far-field by a lens L_2 with a focal length of 150 mm.

A bandpass filter BP selects photons spectrally at 826.4 ± 1 nm. The wavelength at which the transmission of this filter is at its maximum depends on the angle of the incoming light. We operate the filter at normal incidence to select a wavelength of 826.4 nm. So in this setup frequency degenerate PDC light is generated. If we place filter BP in front of lens L_2, we would select photons of different wavelengths, depending on their transverse momenta. Hence we place the bandpass filter behind this lens.

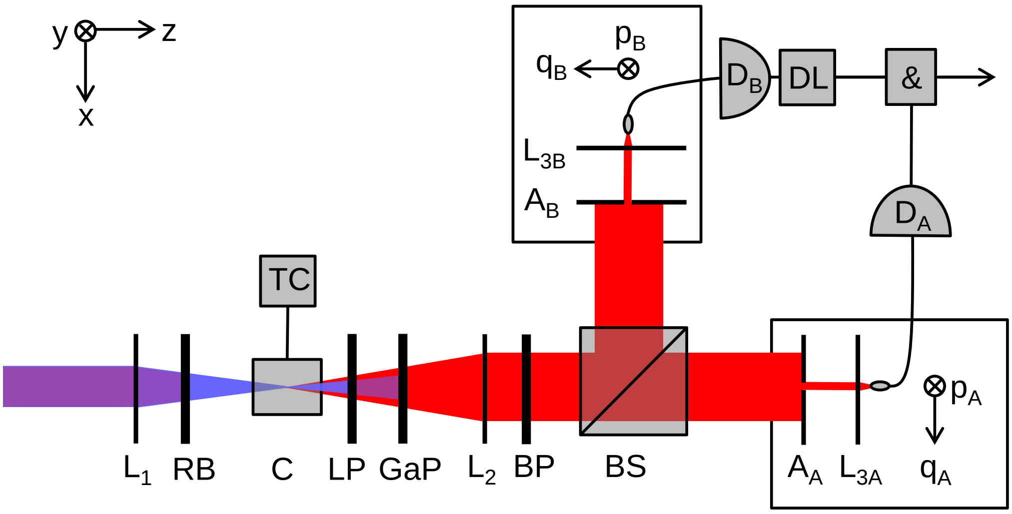

Figure 3.1: *Schematic illustration of the experimental setup. Pump light of 413.2 nm is focused at a PPKTP crystal C by a lens L_1 with a focal distance of 150 mm. The temperature of the crystal is set by a temperature controller TC. Type-1 PDC light is created and the pump light is blocked by a gallium phosphide wafer, GaP. The down-converted light is collected by a lens L_2 with a focal distance of 150 mm. A long-pass filter blocks background light with a wavelength below 720 nm. The PDC light is spectrally selected at 826.4 ± 1 nm by a bandpass filter BP. The down-converted light is sent to two identical detection units by a 50/50 beamsplitter BS. The units are placed on translation stages, which can move in the x- and y-direction. The angular positions of both units are denoted by (p, q). Circular apertures A_A and A_B with a 1 mm diameter select the light spatially. The transmitted photons are collected by lenses L_{3A} and L_{3B}, with a focal length of 11 mm into multi-mode step-index fibers.*

We use a 50/50 beamsplitter BS to send the collected photons to two identical detection units A and B. The beamsplitter is cubic with a 20 mm side length. Both detection units are on the same distance of the beamsplitter. Each detection unit consists of an aperture A, a lens L_3 and one end of a fiber, all placed on a translation stage. The stage can move in the x- and y-direction and is computer-controlled by a Newport motion controller. The aperture is circular with a diameter of 1 mm. It is placed in the Fourier plane of lens L_2, i.e. at a distance of 150 mm behind the lens. All distances are measured with a calliper. We have taken the refractive indices into account to determine the optical path length of the light. The aperture filters the PDC photons spatially. The lens L_3 has a focal length of 11 mm and is placed 40 mm behind the aperture A. The spatially selected photons are collected by lens L_3 into a multi-mode step-index fiber. The end of the fiber is placed in the focal point of lens L_3. The fiber has a core diameter of 50 μm. The fibers are connected to single photon avalanche diodes (SPADs) D_A and D_B. The signals of both counters are connected to an AND gate with a time window of 1.5 ns to measure the coincidence counts.

We take $(x, y, z) = \mathbf{0}$ at the center of the crystal. The x- and y-position of an aperture determines which photons arrive at a detector. A photon is detected in the Fourier plane at a position (x, y). Imagine a line from the center of the crystal to point $(x, y, 150\text{ mm})$, at the position of lens L_2. This line creates a certain angle with the optical axis. We shall denote this angle by (q, p). (We have $q \approx \tan(q) = \frac{x}{150}$ rad, with x in mm.) The corresponding angular positions of the detection units A and B are presented by $(q_A, p_A)$and (q_B, p_B) respectively.

The setup can be used to measure several properties of PDC light. The structure of the PDC light itself can be determined by measuring single photon counts of a detector while scanning the corresponding detection unit. A single photon pair consist of two photons 1 and 2 that are anti-correlated in 'transverse momentum'. (Note that equation 1.2 also holds outside the crystal.) These photons can be detected as coincidence counts if the detection units measure at opposite positions:

$$(q_A, p_A) = -(q_B, p_B).$$

An m-double photon pair consist of m identical single photon pairs. The photons in each pair are anti-correlated in momentum, but the photons of different pairs can be either correlated or anti-correlated. If the detection units measure at the same position

$$(q_A, p_A) = (q_B, p_B),$$

m-double photon pairs can be detected whereas single photon pairs can not be detected if $(q_A, p_A) \neq (0, 0)$.

Part of the coincidence counts are due to photons that do not belong to the same (*m*-double) pair. We name these uncorrelated coincidence counts. These counts are due to both background radiation and photon pairs in the same temporal mode in the PDC light itself. The uncorrelated coincidence count rate is on average equal to the coincidence count rate between successive pulses. To measure this last rate, counter D_B is connected to a digital delay line DL. We use it to delay the signal from D_B by 12 ns, which is the time between successive pulses. We measure coincidence count rates with a delay line of 0 and 12 ns, R_{cc}^{0ns} and R_{cc}^{12ns} respectively. The coincidence count rate due to (*m*-double) photon pairs, can be calculated from these as $R_{cc} := R_{cc}^{0ns} - R_{cc}^{12ns}$.

3.2 Alignment

In this section we describe our alignment procedure. We use two lasers to align the setup: the titanium sapphire laser and a laser diode, operating at 826 nm. We put the infra-red laser at the position of one of the multi-mode fibers. (See figure 3.1.) First of all, we align the blue laser with respect to the optical table using two pinholes. Then we align two diaphragms Di_1 and Di_2 with respect to the blue laser. We put these at fixed positions: Di_1 before lens L_1 and Di_2 between lens L_2 and the beamsplitter. We use these diaphragms to align the rest of the setup. We close these diaphragms and use a beam profiler to see if the diffraction patterns of the blue/infra-red laser are symmetrical. After trying many alignment procedures, we found this method to be the most accurate.

We use the laser diode to align both detection units with respect to the diaphragms. Concerning the lenses, we use the fact that the propagation direction of the laser beam will change if it does not pass through the center of the lens. We align L_1 using Di_1 and the infra-red laser and we align L_2 using Di_2 and the blue laser.

We use an internal reflection in the beamsplitter to align its rotation. It is important that the laser-beam enters the beamsplitter in the middle since the scanning range of 14 mm is not far from the size of the beamsplitter (20 mm). We use the infra-red laser to adjust the x- and y-position. That is, we make sure the infra-red laser passes the beamsplitter within a scanning range of 14 mm. The x- and z-position of the beamsplitter are coupled since the distance to the apertures A_A and A_B needs to be the same. We align the z-position of the beamsplitter such that these distances are the same. We use aperture A_B to align the z-position of detection unit B. (We remove lens $L_{3\,B}$.)

A rotation of the crystal with respect to the optical axis, causes a translation of the laser beam. Although hindered by the speckle of the crystal, we use diaphragm Di_2 to put the crystal straight. Furthermore, the crystal seems to be damaged at certain locations. We use a CCD camera to find a non-scattering spot in the crystal.

After this procedure, everything should be aligned. However, we face the following problem: the PDC rings that we measure with both detectors are asymmetrical. This is shown in figure 3.2. The photon counts per second are measure as a function of the angular positions q_A and p_A at a crystal temperature $T = 48°C$.

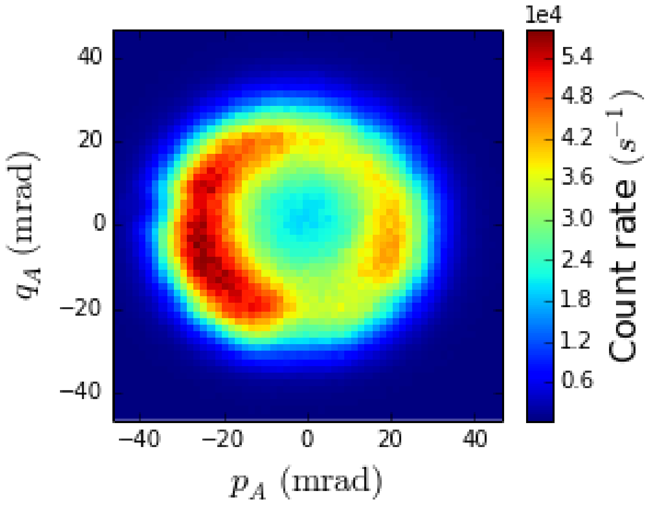

Figure 3.2: *Photons counts per second measured with detection unit A as a function of* q_A *and* p_A *at a crystal temperature* $T = 48°C$*.*

With the CCD camera we measure perfectly symmetrical PDC rings at all positions in the setup before the detection unit. We thus conclude that something goes wrong in the detection.

If the fiber is translated with respect to lens L_3 in a certain direction, the intensity of the PDC ring increases on the side to which the fiber is moved. On the other side of the PDC ring the intensity decreases. We use this to align the fiber; We position the fiber such that the PDC ring becomes symmetrical. Our hypothesis is that the fiber is positioned on the optical axis if it is aligned.

The asymmetry is illustrated in figure 3.3. Detection unit A is used to create 1-dimensional scans. We set $T = 48°C$, such that non-collinear down-conversion occurs. This causes the PDC light to be ring-shaped in the far field. Then the intensity of the PDC light is higher for larger $(q_{\mathrm{A}}, p_{\mathrm{A}})$-positions, compared to collinear-down-conversion. Thereby the asymmetry can be observed more clearly. p_{A} is set at zero and the photon counts are measured as a function of q_{A}. Concerning the measurement in figure 3.3(a), the fiber is aligned. In the figure 3.3(b), the position of the fiber is translated over 1.3 ± 0.3 μm in the positive x-direction with respect to the optical axis of lens $\mathrm{L}_{3\,\mathrm{A}}$ compared to its position in figure 3.3(a). In we compare figure (b) to (a) we observe that the photon count rate increases for positive q_{A} detection positions (which corresponds to positive x positions). For negative q_{A}-positions less photons are detected and at $x = 0$ the photon count rate is not changed.

In the mis-aligned setup the collection efficiency is dependent on the detection position; at the detection position of the positive peak the collection efficiency is higher compared to the the position of the negative peak. For the aligned setup we can not draw a conclusion about the position dependence of the collection efficiency. However, since the collection efficiency at the position of the positive peak increases significantly by changing the fiber position, leaving the efficiency at $q_{\mathrm{A}} = 0$ unchanged, our hypothesis is that the collection efficiency decreases if $|q_{\mathrm{A}}|$ increases in the aligned case.

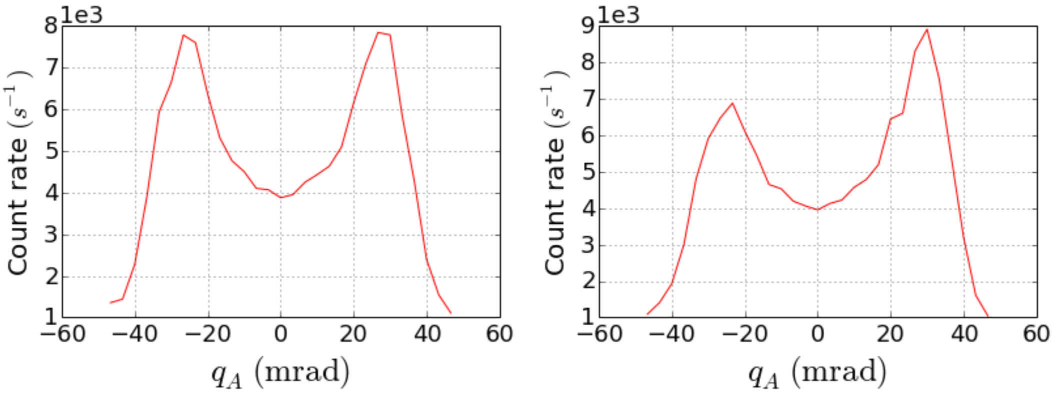
(a) Aligned

(b) Mis-aligned

Figure 3.3: *Photons count rate measured with detection unit A as a function of* q_{A}*.* p_{A} *is set at zero. We set* $T = 48°C$ *such that non-collinear down-conversion occurs and we use a pump power of 45 mW. In figure (a) the fiber is aligned. In figure (b) the position of the lens is translated over* 1.3 ± 0.3 μm *in the positive* x*-direction with respect to the optical axis compared to its position in figure (a).*

In order to verify the distances of the translations of the fiber with respect to the optical axis, we measure them with an indicator. We observe that a fiber translation of 5 μm is sufficient to make one half of the ring disappear. We use iterated 1-dimensional line scans at a crystal temperature of T = 48°C to align the position of the fiber with respect to lens L_3 up to a few μm. This step is crucial since the position of the fiber could not be aligned this precisely with the laser diode and the diaphragms. If the aperture diameter is increased, the same asymmetry effect is observed, albeit less strong. In chapter 4, we shall investigate whether we can explain this asymmetry effect.

Lastly, we align the position of the detection units more accurately by maximising the photon count rate in the origin for collinear down-conversion.

3.3 Characterization of the pump beam

In our experiment we focus a pump beam, consisting of 413.2 nm light at a crystal. In this section we provide information about the shape of the pump beam. This is important, since the properties of the PDC light are determined by the properties of the pump beam.

Let the radius of the pump beam be given by $w(z)$. We measure the radius at the position where the field amplitude drops to $\frac{1}{e}$ of its maximum. If the pump beam is Gaussian, the z-dependence of the radial size is given by

$$w(z) = w_0\sqrt{1+\left(\frac{z-z_0}{z_R}\right)^2}. \tag{3.1}$$

The beam waist w_0 denotes the minimum value of w, that occurs at a position $z = z_0$. The parameter z_R is called the Rayleigh range. At a position $z = z_0 \pm z_R$ apart from the beam waist the radial size is increased to $\sqrt{2}w_0$. For a beam which is symmetric in the x- and y-direction, the area of the cross section is doubled at a distance z_R from z_0.

We have measured the radial size of our pump beam in both the x- and y-direction as a function of the z-position. The position $z = 0$ corresponds to the place where the center of the crystal is placed. In figure 3.4 equation 3.1 is fitted to these widths.

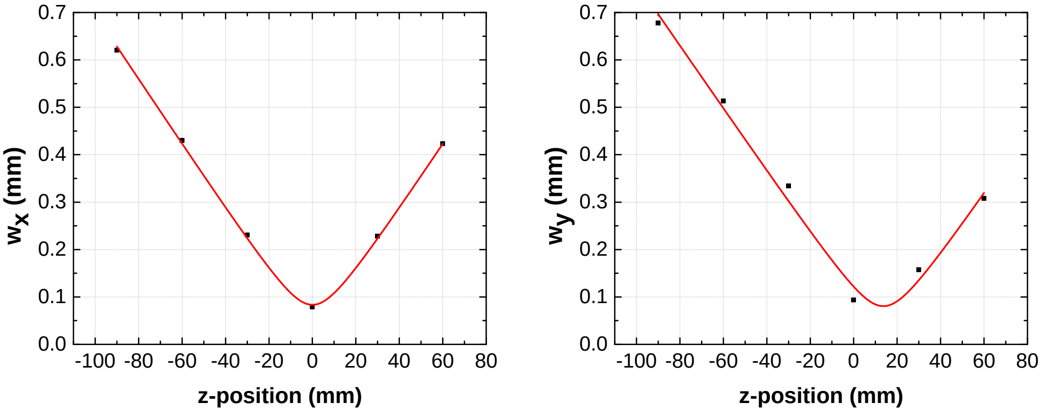

Figure 3.4: *Radial size of the pump beam in the x- and y-direction as a function of z-position. The crystal is placed at $z = 0$. The radius is measured at the position where the field amplitude is $\frac{1}{e}$ of its maximum. Equation 3.1 is fitted to both curves. The fit parameters are $w_{0,x} = 0.083 \pm 0.007$ mm, $z_{0,x} = 0.0 \pm 0.6$ mm, $z_{R,x} = 12 \pm 1$ mm, $w_{0,y} = 0.08 \pm 0.04$ mm, $z_{0,y} = 13 \pm 3$ mm and $z_{R,y} = 12 \pm 3$ mm.*

The fitted beam waists and Rayleigh ranges in the x- and y-direction are $w_{0,x} = 0.083 \pm 0.007$ mm, $w_{0,y} = 0.08 \pm 0.04$ mm, $z_{R,x} = 12 \pm 1$ mm and $z_{R,y} = 12 \pm 3$ mm. Since the x- and y-parameters are the same within the measurement error, the shape of the beam is the same in x- and y direction. Yet the positions of the beam waists are not the same: We find $z_{0,x} = 0.0 \pm 0.6$ mm and $z_{0,y} = 13 \pm 3$ mm. Hence, at the center of the crystal the beam is oval-shaped. Consequently the PDC light will not be circular either.

Chapter 4

Asymmetry of detected PDC light

In section 3.2 we made the observation that if the position of the fiber of a detection unit is translated with respect to the optical axis in a certain direction, the intensity on this side of the PDC light increases. On the opposite side the intensity decreases. In this chapter we shall discuss possible explanations for this effect.

4.1 Does the deviation from the Fourier plane explain the asymmetry?

In order to collect the PDC light in the Fourier plane of lens L_2, the aperture of a detection unit should be placed in this plane. By mistake, our apertures are positioned approximately 3 mm behind this plane. In this section we shall investigate whether this can explain the asymmetry in the alignment.

For simplicity, we consider a Gaussian beam of PDC light propagating from the crystal in the z-direction. We assume all of the phase-matched PDC light originates from the focal point of lens L_2; a distance $f_2 = 150$ mm in front of this lens. Furthermore we assume this focal point corresponds with the end position of the crystal. We take the beam waist of our Gaussian beam, w_1 equal to the beam waist of the pump beam: $w_1 = 85\mu$m. (See section 3.3.) At the beam waist the radius of curvature R is taken to be ∞.

The Fourier plane is the x-y plane a distance f_2 behind lens L_2. We consider aperture A to be positioned 3 mm behind the Fourier plane with a diameter $d = 1$ mm. In figure 4.1 a schematic illustration of the wave fronts of the Gaussian beam is shown.

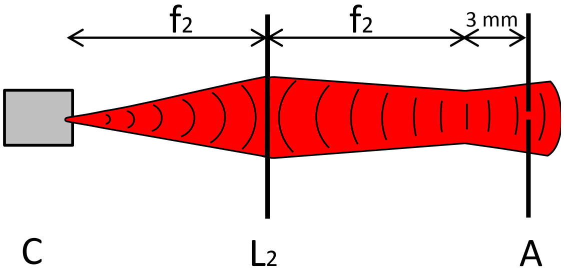

Figure 4.1: *Schematic illustration of the wave fronts of a Gaussian beam propagating from the crystal C. Lens* L_2 *has a focal distance of* $f_2 = 150$ *mm. The end of the crystal is placed in the focal point of lens* L_2 *and we assume the Gaussian beam propagates from this point. Furthermore, we assume the aperture A to be positioned 3 mm behind the Fourier plane.*

In the Fourier plane the wave fronts of the Gaussian beam are parallel to the plane itself. If the aperture would be positioned in the Fourier plane, the (classical) direction of the light entering the detection mechanism does not depend on the x and y detection position. Since we consider the aperture A to be placed behind the Fourier plane, the position of detection is related to the (classical) direction of the light entering the detection unit. This is because the wave fronts are not parallel to the aperture plane. (See figure 4.1.)

Without loss of generality we assume that the position of the fiber is translated in the positive x-direction with respect to the optical axis. This is the case for measurement on the right in figure 3.3.

Let α be the angle of the PDC light with respect to the optical axis in the plane of the aperture. For detection at positive x-positions, α is positive, since the aperture is placed behind the Fourier plane. This causes the focal point to be translated in the positive x-direction with respect to the optical axis. Hence, more light could be detected if the fiber is translated in the positive x-direction as well. This is schematically shown in figure 4.2b. For detection at negative x-positions, the focal point is translated in the negative x-direction. If we translate the fiber in the positive x-direction, we move it away from the focal point. Hence, it is possible to detect less light. This is shown in figure 4.2c. Both are in agreement with the measurements in the right figure in 3.3.

If we compare the peaks for positive x-positions in figure 3.3, we observe that more light is detected if the fiber is translated in the positive x-position. This means that we did not measure all of the PDC light for positive x-positions in the aligned case. Regarding detection at $x = 0$ in figure 4.2a, it is possible to detect less light compared to the case where fiber and lens are aligned. However, this is not what we observe in figure 3.3.

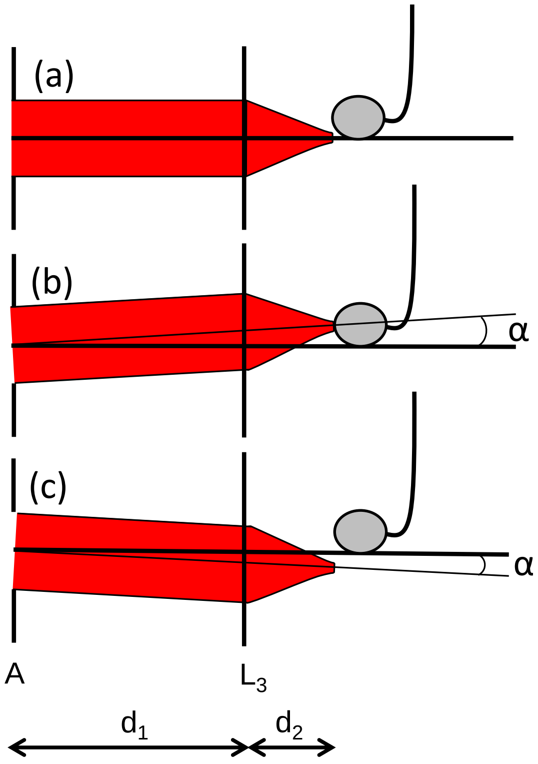

Figure 4.2: *Schematic illustration of the detection mechanism, if the position of the fiber is translated in the positive x-direction with respect to the optical axis and if the position of the aperture is behind the Fourier plane. The path of the PDC light is given for detection at (a) $x = 0$, (b) $x > 0$, (c) $x < 0$ The distance between the aperture A and lens L_3 is given by $d_1 = 40 \pm 2$ mm. The distance between lens L_3 and the fiber coupler, d_2 equals the focal distance of lens L_3, which is 11 mm.*

The deviation from the Fourier plane can explain the origin of the asymmetry. In order to know if this is realistic, we will quantify the influence of this effect in the next section.

4.2 Quantifying the deviation

Let x_f denote the x-coordinate of the focal point. In the previous section we have seen that x_f is a function of the detection position x_d:

$$x_f(x_d) = (d_1 + d_2)\tan\alpha \approx 50 \cdot \tan\alpha, \tag{4.1}$$

where α denotes the angle of the PDC light with respect to the optical axis in the plane of the aperture. We shall compute x_f at the detection position of the peaks in order to know if all light passing the aperture enters the fiber at this detection position.

First we compute α as a function of detection position: $\alpha(x)$. Because we consider Gaussian PDC light propagating from the crystal, the beam that propagates from lens L$_2$ is Gaussian as well. The radius of curvature of this beam is given by

$$R(z) = z\left(1 + \left(\frac{z_\mathrm{R}}{z}\right)^2\right). \tag{4.2}$$

The position $z = 0$ corresponds to the Fourier plane and z_R is the Rayleigh range, given by

$$z_R = \frac{\pi\omega_2^2}{\lambda}. \tag{4.3}$$

In this equation ω_2 denotes the radial beam size in the Fourier plane and λ denotes the wavelength of the PDC light. We are interested in the radius of curvature at the position of the aperture; at $z = 3$ mm. In appendix 7.3 we compute z_R using ray transfer matrices: $z_R \approx 8.2 \cdot 10^2$ mm. We use equation 4.2 to compute the radius of curvature at $z = 3$ mm:

$$R := R(3\text{ mm}) \approx 2.2 \cdot 10^5\text{ mm}.$$

For each detection position x_d we can compute the angle of the PDC light α, according to

$$\alpha = \tan^{-1}\left(\frac{x_d}{R}\right) \approx \frac{x_d}{R}.$$

By equation 4.1 we have

$$x_f(x_d) = \frac{(d_1 + d_2)x_d}{R}.$$

The peaks in figure 3.3 correspond to $x_d \approx \pm 4$ mm. For these detection positions, we have $x_f(\pm 4\text{ mm}) \approx \pm 0.91\mu$m. This means that the focal point is translated by only 0.91 μm at the detection position of the peaks with respect to $q_A = 0$. We will now compute if this translation causes part of the light not to enter the fiber.

The beam width of the focus is diffraction limited. This is because the spatially selected light consists of one spatial mode using an aperture diameter $d = 1$ mm. See [1, paragraph 4.2.1]. The radial width is therefore given by

$$w = \frac{1.22\lambda d_2}{d} \approx 11\ \mu\text{m}.$$

The wavelength of the PDC light is denoted by $\lambda = 826.4$ nm. The core diameter of the fiber equals 50 μm. So if the focal point is translated over 0.91 μm, all PDC light will be detected. Therefore we conclude that the deviation of 3 mm from the Fourier plane cannot cause the asymmetry observed in the experiment. (Note that we approximate the PDC light by a Gaussian beam. We assume that this approximation qualifies to describe how the PDC light is collected.)

At this point the observed asymmetry is not understood. In section 3.2 we have seen that the collection efficiency can be increased/decreased by changing the fiber position. In descriptions of the experiment the collection efficiency is assumed to be 100 %. (The part of the setup behind the aperture is assumed to serve as a bucket detector.) This assumption does not hold. Furthermore the asymmetry effect depends on the type of fiber and seems to decrease if a 62.5 μm graded-index fiber is used. We will illustrate this is the next section.

4.3 Detecting PDC light with graded-index fiber

In figure 3.3 the photon counts are measured with detection unit A as a function of q_A for two fiber positions. For these measurements a step-index fiber with a core diameter of 50 μm is used. In this section we present the same measurements with a 62.5 μm *graded-index* fiber.

Figure 4.3 compares the photon counts measured with detection unit A as a function of q_A for two fiber positions. We use both a step- and a graded-index fiber. Note that the position of the peaks of the PDC light in figure 3.3 and 4.3 are equal since T is set to $48°C$ for both measurements. (The position of the peaks in figure 3.3 is used in the computation of section 4.2.)

Surprisingly, the count rates for detection positions $q_A \neq 0$ are higher if a graded-index fiber is used, compared to a step-index fiber. For $q_A = 0$ the count rates are similar. This suggest that for $q_A \neq 0$, part of the PDC light is detected with a graded-index fiber, but is not detected with a step-index fiber. We would not expect this, since all of the PDC light should already be detected, using a step-index fiber.

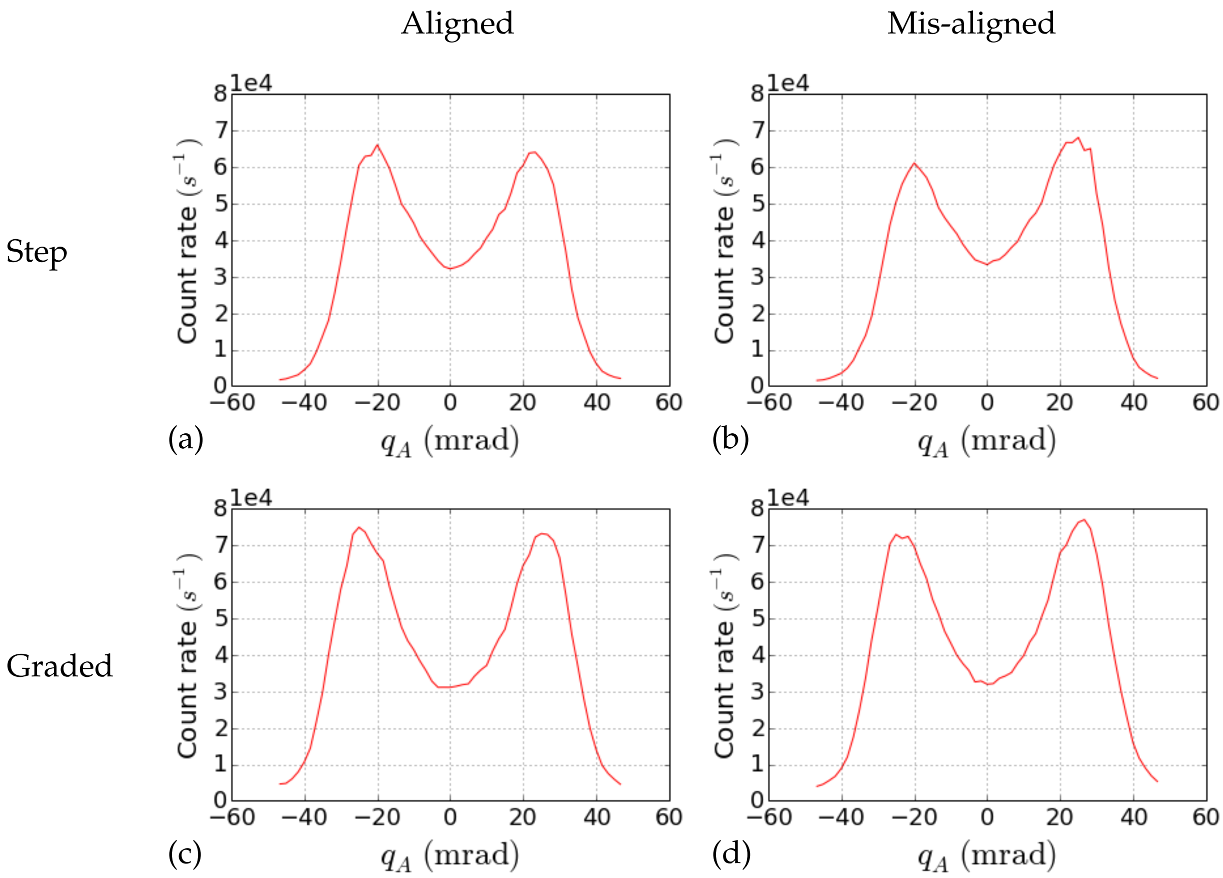

Figure 4.3: *Photon count rate measured with detection unit A as a function of* q_A*, with* $p_A = 0$*. We set* $T = 48°C$ *such that non-collinear down-conversion occurs and we use a pump power of 60 mW. In the figures on the left, the fiber is aligned. In the figure on the right the position of the lens in translated over* 1.3 ± 0.3 μm *in the positive* x*-direction with respect to the optical axis. In the upper figures a step-index fiber is used. The measurements in the lower figures are done with a graded-index fiber.*

Furthermore, the asymmetry effect is less strong for the graded-index fiber, compared to the step-index fiber. The difference in photon count rate between both peaks is lower for the graded-index fiber. Somehow, the step-index fiber is more sensitive to measurement at $q_A \neq 0$.

As we concluded at the end of section 3.2, in the mis-aligned case the collection efficiency depends on the angular detection position q_A. Now that we can compare step and graded-index fibers, we know more about the position dependence of the efficiency in the aligned case. One of the following two statements should hold for the measurement where the fibers are aligned:

1. For the step-index fiber, the collection efficiency is higher at $q_\mathrm{A} = 0$ compared to the peak positions.
2. For the graded-index fiber, the collection efficiency is higher at the peak positions compared to $q_\mathrm{A} = 0$.

Namely, if both statements would not hold, we should measure higher or equal photon count rates at the position of the peaks for the step-index fiber compared to the graded-index fiber, since the photon count rates of both fibers *are* approximately equal at $q_\mathrm{A} = 0$. Note that we assume that the *detection* efficiency is equal for both fibers. To exclude that the results can be explained by dirty or damaged fibers we repeated the experiment with new fibers and obtained identical results.

Since the collection efficiency can be increased at the peak position in the aligned setup by changing the position of the fiber, but not at $q_\mathrm{A} = 0$, it is likely that the collection efficiency at the peak-positions is lower compared to $q_\mathrm{A} = 0$. This holds for both the step- and the graded-index fiber. In this case statement 2 does not hold, hence statement 1 must hold. Our hypothesis is that the collection efficiency is higher at the peak positions compared to $q_\mathrm{A} = 0$ for both the step- and the graded-index fiber. This difference is higher for the step-index fiber.

In figure 4.4 we plot the photon count rates of the graded-index fiber minus the count rates of the step-index fiber. Around $q_\mathrm{A} = 0$ less photons are detected with the graded-index fiber. Because there is more signal than noise, the collection efficiency around $q_\mathrm{A} = 0$ is lower for the graded-index fiber compared to the step-index fiber.

At the other detection positions, the count rates and therefore the collection efficiency of the graded-index fiber is higher compared to the step-index fiber. The count rate in figure 4.4 is not symmetrical around $q_\mathrm{A} = 0$. This is due to the fact that the alignment in figure 4.3(a)&(c) is not perfect. This argument does not explain the asymmetry in figure 4.4(b). Our hypothesis is as follows: Since the fiber is moved in the positive q_A-direction, the collection efficiency is suppressed less for positive q_A-positions and more for negative q_A-positions. This effect is stronger for the step-index fiber.

Version of 31-01-2015– Created June 24, 2015 - 17:18

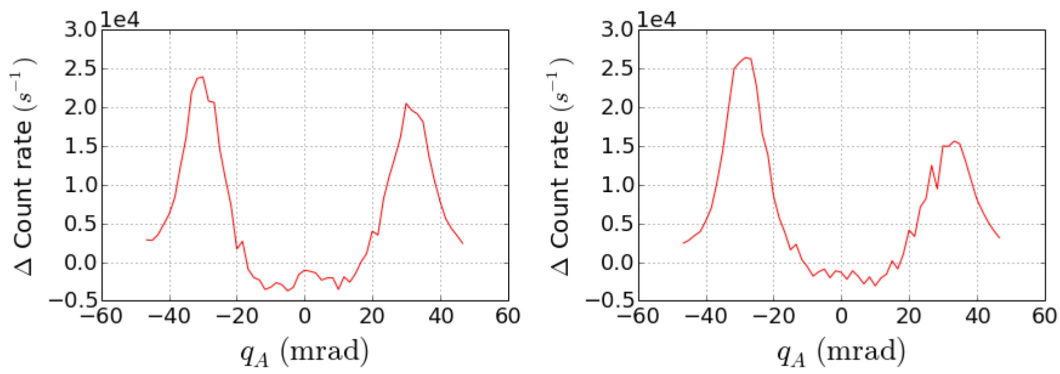
(a) Aligned

(b) Mis-aligned

Figure 4.4: *The difference of the photon count rate for the graded and step-index fiber measured with detection unit A is shown as a function of* q_A *with* $p_\mathrm{A} = 0$ *for both the aligned and the mis-aligned setup. The data from figure 4.3 (a)&(b) is subtracted from the data from figure 4.3 (c)&(d) respectively.*

It is more interesting to know the relative change of the photon count rate as a function q_A, since this equals the percentage change of the collection efficiency as a function of q_A. The relative change is shown in figure 4.5.

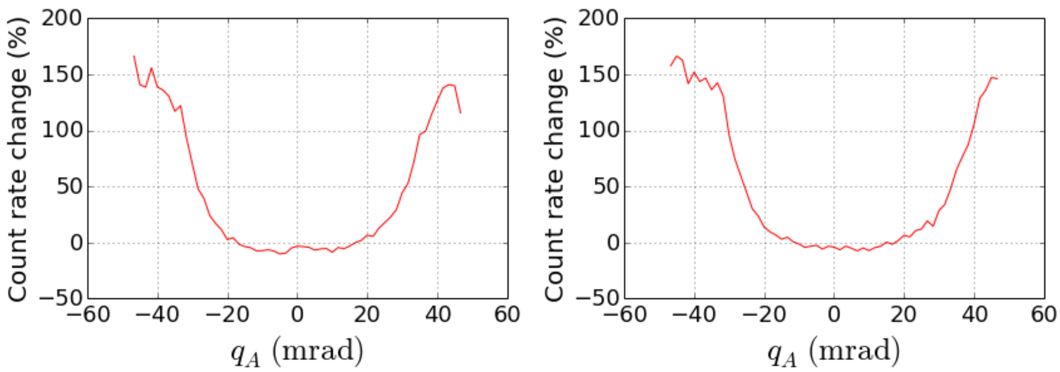
(a) Aligned

(b) Mis-aligned

Figure 4.5: *The percentage change of the photon count rate measured with a graded-index fiber compared to a step-index fiber, using detection unit A, is shown as a function of* q_A *with* $p_\mathrm{A} = 0$ *for both the aligned and the mis-aligned setup. The data from figure 4.3 is used.*

At the position of the peaks, which is roughly at $|q_\mathrm{A}| = 25$ mrad the collection efficiency is improved by 20% by using a graded-index fiber. At higher $|q_\mathrm{A}|$ positions the collection efficiency increases even more. This explains why the peaks of the PDC light are observed at smaller detection positions $|q_\mathrm{A}|$ when a step- compared to a graded- index fiber is used. Note that there is no clear difference between the aligned and the misaligned case.

We conclude that the asymmetry and the collection efficiency depends on the alignment and the type of fiber used. However, the asymmetry is not understood.

Chapter 5

Results

In this chapter we provide our experimental results using step-index fibers despite the higher collection efficiency for graded-index fibers. This is because of historical reasons.

5.1 Intensity distribution PDC light

Figure 5.1 shows the intensity distribution of PDC light measured with one detection unit, i.e. the measured single photon count rate as a function of q and p. Measurements are shown for a pump power of 35 mW and crystal temperatures of $T = 55°C$ (left) and $T = 50°C$ (right), which corresponds to nearly-collinear and non-collinear down-conversion respectively. We use both detection unit A (top) and B (bottom). Since we are using a 50/50 beamsplitter, the photon count rates at each detection position should in principle be the same for both units.

Concerning the translation stages of the detection units, we use a step size of 0.10 mm (0.67 mrad) and a scanning range of ± 7.0 mm (± 47 mrad) The diameter of both apertures is 1 mm, which is large enough to resolve the structure in the far-field of the PDC source.

We have used an iterative procedure to align the fiber position with respect to lens L_3, such that the intensity distributions are approximately symmetrical in the x- and y-direction. We recall that a fiber position of 1.3 μm has an enormous effect on the symmetry of the intensity distribution. (See figure 3.3.) With the translation tables used in our experiment, it is impossible to align the fibers such that perfect symmetry will be observed. This is why we still see some asymmetry in figure 5.1. Even after the best possible alignment, the collection efficiency is asymmetrical around $(q, p) = (0, 0)$. In the experiment we also observe that the alignment degrades during experiments of several hours. We believe that the origin of this effect is that the position of the laser beam is not stable over time and if this position changes, the fiber positions should be adjusted as well.

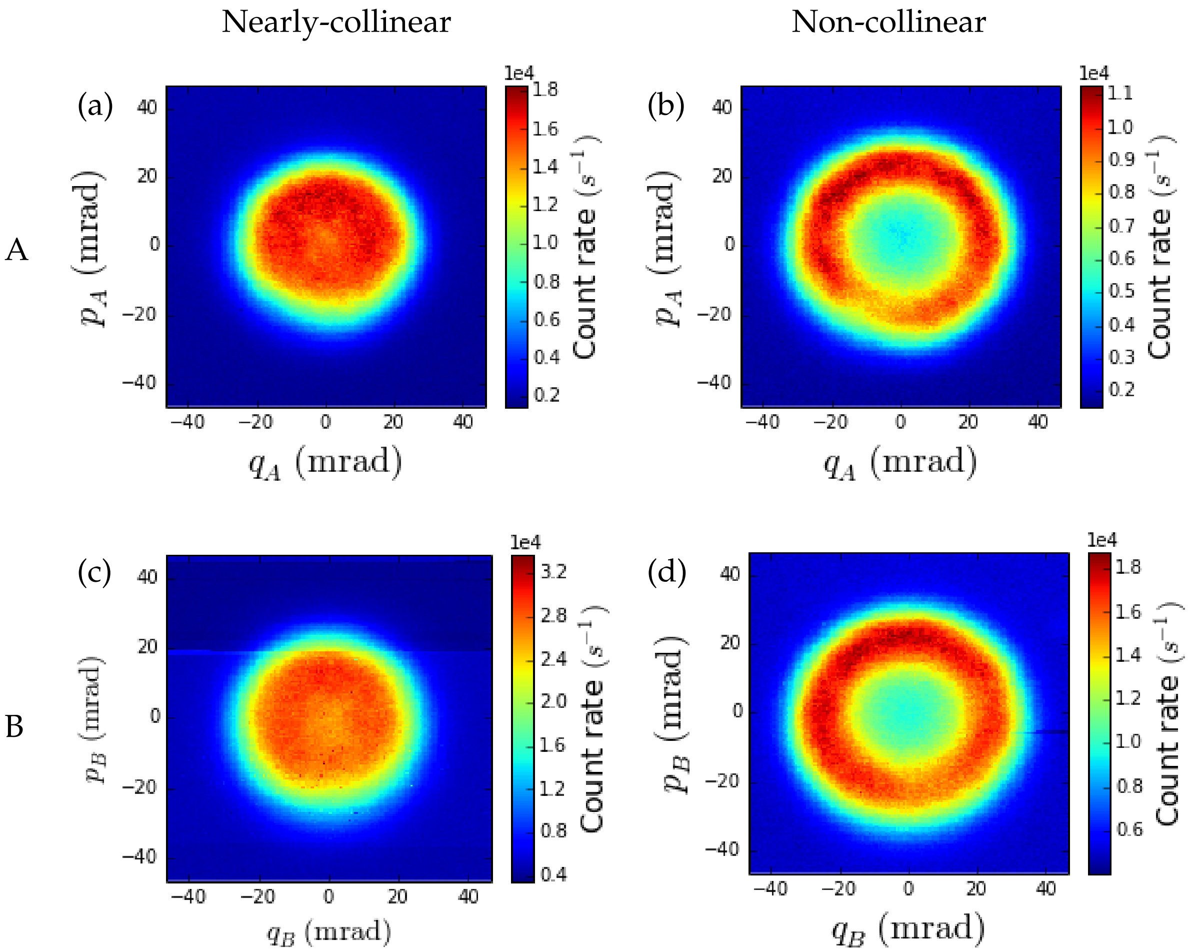

Figure 5.1: *Measured photon count rates for nearly-collinear (left) and non-collinear (right) down-conversion, for a crystal temperature equal to* $T = 55°C$ *and* $T = 50°C$ *respectively. Data is shown for detection unit A (top) as well as B (bottom). The step size and scanning range of all four translation stages equals 0.10 mm (0.67 mrad) and ± 7.0 mm (± 47 mrad) respectively. The pump power equals 35 mW.*

We observe that the asymmetry is different for unit A and B although they simultaneously record light from the PDC source. This is because the alignment of the fiber of unit A is (obviously) different from the alignment of the one of unit B. This confirms our notion that the asymmetry is caused by the detection unit and not by the other parts of our setup.

The power output of the laser is not stable during the time span of our measurement. This can be observed in figure (c). During the measurement the laser power suddenly increases. Therefore the photon count rate for detection positions below $p_{\mathrm{B}} = 20$ mrad are higher compared to the rate above this position. The instability of the laser power explains the difference in photon count rate between the measurements performed by unit A and B.

5.2 Coincidences

In this and the following section we present measurements of R_{cc}, the coincidence count rate due to (m-double) photon pairs. (See the end of section 3.1.) We will compare our data to similar measurements for a 5 mm PPKTP crystal, see [1, paragraph 5.4.2].

Figure 5.2 shows the measured coincidence rate as a function of q_{A} and q_{B} on a logarithmic scale. p_{A} and p_{B} are set to zero. The measurement is carried out for two crystal temperatures $T = 60^\circ$ (figure (a)) and $T = 54^\circ$ (figure (b)), which corresponds to collinear and nearly-collinear down-conversion. Note that the temperatures in the previous session are slightly lower because this causes the asymmetry to be observed more clearly. The pump power is 66 mW and the step-size and scanning range for the two translation stages equals 0.20 mm (1.3 mrad) and ± 6.0 mm (± 40 mrad) respectively.

For detection positions $q_{\mathrm{A}} = -q_{\mathrm{B}}$ photons in the same temporal mode that are anti-correlated in momentum can be measured. These photons are part of a single or an m-double photon pair with $m \in \mathbb{N}_{\geq 2}$. For two photons in a photon pair, the probability for one photon to arrive at detector A and the other to arrive at detector B equals $\frac{1}{2}$ for a 50/50 beamsplitter. The probability for an SPAD to click when n photons arrive at the detector, is given by $1 - (1 - \eta)^n$, where η is the detection efficiency. It follows that the probability to detect two anti-correlated photons from a single photon pair equals $\frac{1}{2}\eta^2$.

For angular positions $q_{\mathrm{A}} = q_{\mathrm{B}}$ photons in the same temporal mode that are correlated in momentum can be measured. If $q_{\mathrm{A}} = q_{\mathrm{B}} \neq 0$, these photons must be part of an m-double photon pair. Again, the probability to detect two correlated photons from a double photon pair equals $\frac{1}{2}\eta^2$.

For the remaining detection positions where $q_{\mathrm{B}} \notin \{q_{\mathrm{A}}, -q_{\mathrm{A}}\}$, no coincidences from PDC photons will be detected. This is because all PDC photons are not quantum correlated in momentum different from the two options described above. Besides PDC photon pairs, we also measure uncorrelated coincidence counts, for which we correct. (See the end of section 3.1.) Since R_{cc}^{12ns} is merely an indication of the uncorrelated coincidence counts, we do see some counts for the remaining detection positions.

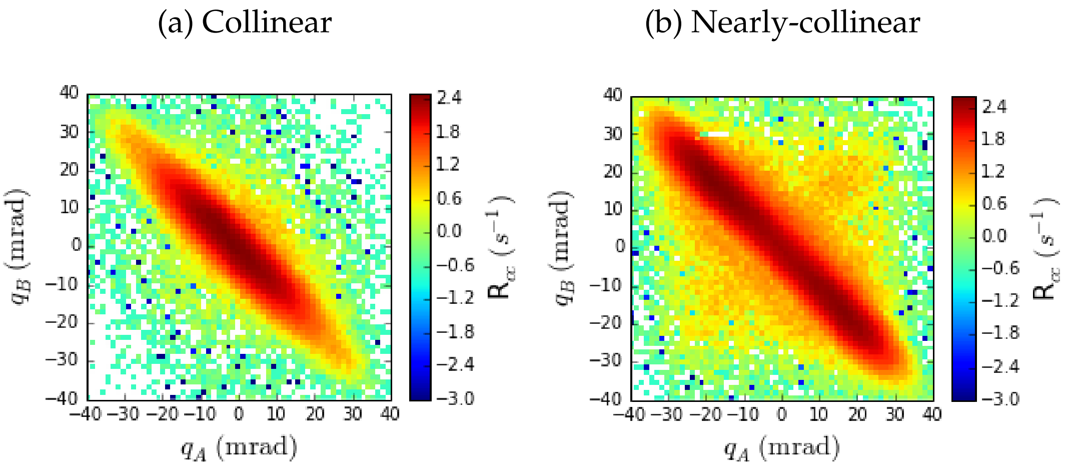
(a) Collinear

(b) Nearly-collinear

Figure 5.2: *Log of R_{cc}, the coincidence count rate due to (m-double) photon pairs, measured as a function of q_A and q_B. p_A and p_B are set to 0. The measurement is done for two crystal temperatures: (a) $T = 60°$ and (b) $T = 54°$, which corresponds to collinear and nearly-collinear down-conversion respectively. The step size and scanning range of the two translation stages is 0.20 mm (1.3 mrad) and ± 6.0 mm (± 40 mrad) respectively. The pump power equals 66 mW.*

In figure 5.2 the diagonal represents the measurement of correlated photon pairs and the anti-diagonal corresponds to the measurement of anti-correlated photon pairs. Since there are more single photon pairs, compared to m-double photon pairs, R_{cc} is higher on the anti-diagonal. We have plotted the logarithm of R_{cc} to be able to see the counts on the anti-diagonal, which is not very clear otherwise.

For a 5 mm PPTKP crystal $|\kappa|t$, the single-pass gain, is estimated as 0.58, for a 75 mW pump power. (See [1, Page 80].) We use this result to compute the single-pass gain for the measurement in figure 5.2, i.e. for a 2 mm crystal and a 66 mW pump power. We recall that

$$|\kappa|t = |\chi^{(2)}_{z,z,z}|\gamma t,$$

where $\chi^{(2)}_{z,z,z}$ is the (z,z,z)-component of the non-linear susceptibility $\chi^{(2)}$, γ indicates the strength of the pump power and t is the time it takes the pump beam to travel through the PPKTP crystal. (See section 2.3.) The non-linear susceptibility is equal for both crystals. The values of γ and t are a factor $\frac{75}{66}$ respectively 2.5 lower for the experiment with the 2 mm crystal. Therefore $|\kappa|t$ is estimated as 0.20 for the experiment in figure 5.2. When we compare figure 5.2 to [1, figure 5.3] two differences can be noted.

1. The count rates are higher for the 5 mm crystal. In view of equation 2.22 this is expected since $|\kappa|t$ is higher for the 5 mm crystal.

2. The fraction of the count rate on the diagonal and the count rate on the anti-diagonal is larger for the 5 mm crystal compared to the 2 mm crystal. This is because, the probability to find a *j*-double photon pair compared to a single pair increases if $|\kappa|t$ increases.

5.3 Four-photon peak

Now we consider R_{cc} at detection positions $q_{\mathrm{A}} = -q_{\mathrm{B}}$ and $p_{\mathrm{A}} = p_{\mathrm{B}} = 0$, which corresponds to the anti-diagonal in figure 5.2. That is, we regard the coincidence counts due to photon pairs that are *anti*-correlated in momentum. This is shown in figure 5.3(a) and 5.3(b) for crystal temperatures $T = 60°C$ and $T = 54°C$ respectively. We note that for a 5 mm crystal a clear peak centered at $q_{\mathrm{A}} = -q_{\mathrm{B}} = 0$ is observed in [1, figure 5.4 and 5.5]. The origin of this peak is not well understood. In this section we perform similar data processing to see if this peak can be observed for a 2 mm crystal.

Figure 5.3(b) is asymmetrical with respect to $q_{\mathrm{A}} = -q_{\mathrm{B}} = 0$. There are two conditions that can contribute to this asymmetry. The first condition is that the collection efficiency of detection unit A is lower for high q_{A} detection positions compared to low q_{A} positions. The second condition is that detection unit B has a lower collection efficiency for *low* q_{B} positions compared to high q_{B} positions. In view of figure 3.3 it is likely that both conditions contribute.

Most of the coincidence counts in figure 5.2 are due to photon pairs that contain two or four photons, i.e. single and double pairs. If we only take into account the contribution of these photons and exploit the conditions $|\kappa|t < 1$ and $\eta \ll 1$ and assume the intensity distribution of the PDC light in the far field is homogeneous, the coincidence count rate R_{cc} at the anti-diagonal equals

$$R_{cc}(q_{\mathrm{A}}, -q_{\mathrm{B}}) \approx R_p \eta^2 \left(\frac{(|\kappa|t)^2}{4} + \frac{7(|\kappa|t)^4}{12} \right), \text{ for } q_{\mathrm{A}} \neq 0 \text{ and} \tag{5.1a}$$

$$R_{cc}(q_{\mathrm{A}} = -q_{\mathrm{B}} = 0) \approx R_p \eta^2 \left(\frac{(|\kappa|t)^2}{4} + \frac{5(|\kappa|t)^4}{6} \right). \tag{5.1b}$$

(See [1, equation 5.17 and 5.18].) R_p denotes the repetition rate of the pulsed laser. We observe that the contribution of the collinear direction gains importance if $|\kappa|t$ increases.

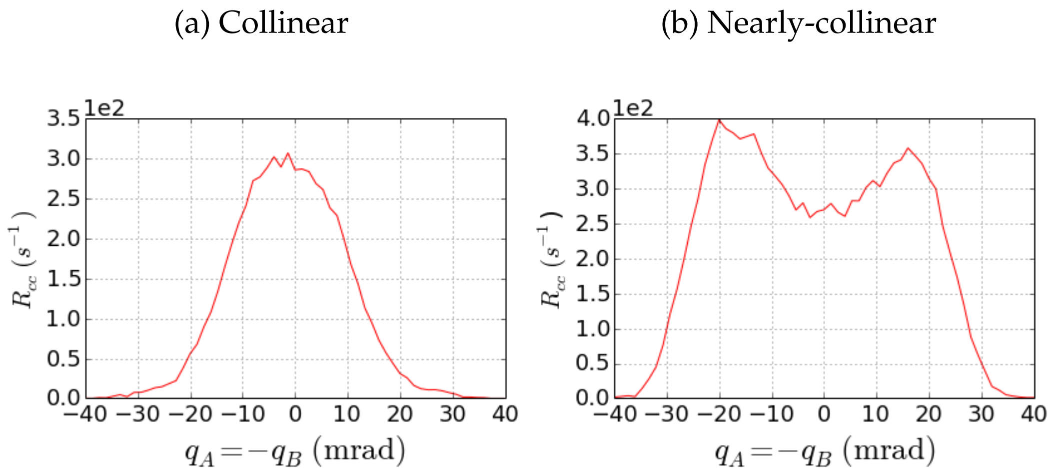

Figure 5.3: *Coincidence count rate R_{cc} due to (m-double) photon pairs, measured as a function of $q_{\mathrm{A}} = -q_{\mathrm{B}}$. p_{A} and p_{B} are set to 0. The measurement is done for two crystal temperatures: (a) $T = 60°$ and (b) $T = 54°$, corresponding to collinear and nearly-collinear down-conversion. The data for these graphs is equal to the data of figure 5.2 on the anti-diagonal.*

For a 5 mm crystal (see [1, figure 5.4 and 5.5]), an extra peak in the collinear direction is found, that is the count rate around $q_{\mathrm{A}} = 0$ is much larger than one would expect based on equation 5.1. To wit, 5.1 predicts this peak to be $\frac{1}{4}(|\kappa|t)^4 \approx 0.03$ larger than the background. The extra peak is attributed to quadruplets, i.e. states $|4_0\rangle$, because R_{cc} at $q_{\mathrm{A}} = 0$ increases quadratically with the pump power and therefore with $|\kappa|t$.

We do not measure this extra peak for the 2 mm PPTKP crystal. At the end of section 5.2 we estimated the single-pass gain as 0.20 for a 2 mm PPKTP crystal and a 66 mW pump power. The pump power needed for a 5 mm crystal to get the same value of $|\kappa|t$ is 26.4 mW. For this pump power the extra peak in the collinear direction is observable. (See [1, figure 5.4].) Note that the probability to create a quadruplet state is equal for the experiment that we carried out with the 2 mm crystal and a similar experiment with a 26.4 mW pump power and a 5 mm crystal, in view of equations 2.22. Since the extra peak is attributed to quadruplet states, it is remarkable that the extra peak is not observed for our experiment with the 2 mm crystal.

Chapter 6

Future directions

As we have seen in paragraph 4.3 the collection efficiency depends on the detection position and decreases for detection positions (q, p) away from the center. This causes the single and coincidence counts to depend on the detection position and may contribute to the extra peak in [1, figure 5.4], since it is found in the collinear direction where the collection efficiency is largest. We believe that this larger collection efficiency in the center cannot explain the extra peak for the 5 mm crystal, since the peak is not observed for the 2 mm crystal. We do note that the understanding of the experiment is based on the assumption that all photons that pass through the aperture are detected with equal probability. Clearly, our results show that this assumption is not valid. We offer some suggestions for further research:

1. Try to repeat the measurements in figure 5.2 and 5.3 with improved alignment.

2. Fit a theoretically predicted count rate to the data in figure 5.3. (For the 5 mm crystal [1, equation 5.21] is fitted to the data in [1, figure 5.4 and 5.5].)

3. Find out what causes the asymmetry effect. Check if a 1.3 μm translation of the fiber with respect to the optical axis causes asymmetry with fibers with a larger core diameters.

4. Redesign the detection units such that the collection efficiency is independent of the detection position. For example one could remove lens L_3 and the aperture A. The fiber or even the detector could be placed in the far field. This requires changes in the rest of the setup as well.

5. Repeat the measurements from chapter 5 with the improved detection mechanism from suggestion 2 (or first with the graded-index fiber). And more importantly, repeat the measurements from chapter 5 with a 5 mm crystal with the improved detection mechanism to see whether the extra peak is apparent.

Chapter 7

Appendix

7.1 Derivation of ordering 2.9 and 2.10 from the Campbell-Hausdorff theorem

Let A and B be operators. The order of an (iterated) commutator in A and B is defined by the number of operators inside the square brackets. For example the iterated commutator $[A,[A,B]]$ has order 3. An (iterated) commutator in A and B is called non-trivial if both operators appear inside the square brackets. A trivial commutator equals 0, since all operators commute with themselves. Each non-trivial iterated commutator in A and B of order n can be written in the form

$$[D_1,[D_2,...[D_{n-2},[A,B]]...]], \tag{7.1}$$

where D_i equals A or B for all $i \in \{1,...,n-2\}$.

Assume $[A,B]=0$. In view of expression 7.1, it follows that all (trivial and non-trivial) commutators in A and B equal 0. According to the Campbell-Hausdorff theorem $\exp(A)\exp(B)=\exp(C)$, with $C=A+B$. (See equation 2.11.) Thus,

$$\exp(A+B)=\exp(A)\exp(B),$$

i.e. 2.9 holds.

Now assume $[A,[A,B]]=[B,[A,B]]=0$. From expression 7.1 it follows that all iterated commutators of order ≥ 3 equal 0. So by the Campbell-Hausdorff theorem we have

$$\exp(A)\exp(B)=\exp\left(A+B+\frac{1}{2}[A,B]\right).$$

Since $A+B$ commutes with $[A,B]$ we can apply equation 2.9 on the right side of 7.1 to obtain

$$\exp(A)\exp(B) = \exp(A+B)\exp\Big(\frac{1}{2}[A,B]\Big).$$

Now, we multiply with $\exp\big(-\frac{1}{2}[A,B]\big)$ on the right. Since $\frac{1}{2}[A,B]$ commutes with $-\frac{1}{2}[A,B]$, we use ordering 2.9 again to obtain

$$\exp\Big(\frac{1}{2}[A,B]\Big)\exp\Big(-\frac{1}{2}[A,B]\Big) = \exp(0) = 1.$$

Hence,

$$\exp(A+B) = \exp(A)\exp(B)\exp\Big(-\frac{1}{2}[A,B]\Big),$$

that is equation 2.10 holds.

7.2 Computation of the state of parametric down-conversion $|\psi_q\rangle$

In this section we show how to compute the state of parametric down-conversion $|\psi_q\rangle$, in case the signal and idler photon are not in the same spatial mode, i.e. $q > 0$.

We have $(a_s a_i)^j|0\rangle = 0$ for all $j \in \mathbb{N}_{\geq 1}$. So

$$\exp\Big(\tanh(|\kappa|t)a_s a_i\Big)|0\rangle = \left(1 + \sum_{j=1}^{\infty}\frac{1}{j!}\Big(\tanh(|\kappa|t)a_s a_i\Big)^j\right)|0\rangle = |0\rangle.$$

Since $(a_s^\dagger a_s + a_i a_i^\dagger)|0\rangle = |0\rangle$, we have $(a_s^\dagger a_s + a_i a_i^\dagger)^j|0\rangle = |0\rangle$ for all $i \in \mathbb{N}_{\geq 1}$. It then follows that

$$\begin{aligned}\exp(-\ln(\cosh(|\kappa|t))(a_s^\dagger a_s + a_i a_i^\dagger))|0\rangle &= \sum_{j=0}^{\infty}\frac{1}{j!}(\ln(\cosh(|\kappa|t)^{-1}))^j|0\rangle \\ &= \cosh(|\kappa|t)^{-1}|0\rangle.\end{aligned}$$

Because $(a_s^\dagger a_i^\dagger)^j|0\rangle = j!|(j_s, j_i)\rangle$ for all $j \in \mathbb{N}$ and by 2.18, we have equation 2.19:

$$|\psi_q\rangle := \exp(\kappa t(a_s^\dagger a_i^\dagger - a_s a_i))|0\rangle = \sum_{j=0}^{\infty}\frac{\tanh(|\kappa|t)^j}{\cosh(|\kappa|t)}|j_s, j_i\rangle.$$

7.3 Computation of z_R

(See [6, paragraph 20.2] for Gaussian beams and ABCD matrices.) A Gaussian beam is characterised by its complex beam parameter, denoted by q. It can be calculated by

$$\frac{1}{q} = \frac{1}{R} - \frac{i\lambda_0}{\pi n w^2}. \tag{7.2}$$

where λ_0 denotes the vacuum wavelength of the beam, R its radius of curvature, n the index of refraction of the medium and w the radial width of the beam. The width is measured at the position where the field amplitude drops to $\frac{1}{e}$ of its maximum. If a Gaussian beam with beam parameter q_1 propagates through an optical system with a certain ray transfer matrix

$$\begin{pmatrix} A & B \\ C & D \end{pmatrix},$$

the outward beam is Gaussian with beam parameter

$$q_2 = \frac{Aq_1 + B}{Cq_1 + D}. \tag{7.3}$$

A medium of length d with constant refractive index and a thin lens with focal length f are described by the ray transfer matrices

$$\begin{pmatrix} 1 & d \\ 0 & 1 \end{pmatrix} \text{ and } \begin{pmatrix} 1 & 0 \\ -\frac{1}{f} & 1 \end{pmatrix}$$

respectively.

For the system we want to perform calculations on, we start with a Gaussian beam with complex beam parameter q_1 at the end of the crystal. It has radius $R = \infty$, vacuum wavelength $\lambda_0 = 826.4$ nm and beam waist $w_1 = 85\mu$m. Since we take the initial point of the Gaussian beam directly after the crystal, we can take $n = 1$. Hence

$$\frac{1}{q_1} = -\frac{i\lambda_0}{\pi w_1^2} \approx -3.6 \cdot 10^{-2} i \text{ mm}^{-1}.$$

We will calculate the complex beam parameter q_2 of the Gaussian beam in the Fourier plane. It has vacuum wavelength $\lambda_0 = 826.4$ nm, and unknown beam waist w_2. We take $n = 1$ as the refractive index of the medium.

The optical system is given by two media of length 150 mm with a thin lens of focal length 150 mm in between. Hence the ray transfer matrix is given by

$$\begin{pmatrix} 1 & 150 \\ 0 & 1 \end{pmatrix} \cdot \begin{pmatrix} 1 & 0 \\ -\frac{1}{150} & 1 \end{pmatrix} \cdot \begin{pmatrix} 1 & 150 \\ 0 & 1 \end{pmatrix} = \begin{pmatrix} 0 & 150 \\ -\frac{1}{150} & 0 \end{pmatrix}.$$

Using equation 7.3, we obtain

$$\frac{1}{q_2} = -\frac{q_1}{150^2}.$$

Since this expression is purely imaginary (because q_1 is), the radius of curvature in the Fourier plane is ∞, as expected. Therefore we have

$$\frac{1}{q_2} = -\frac{i\lambda}{\pi w_2^2} = -\frac{i}{z_R},$$

where z_R denotes the Rayleigh range of the beam (see equation 4.3). We can now compute z_R by

$$z_R = \frac{150^2 i}{q_1} \approx 8.2 \cdot 10^2 \text{ mm}.$$

References

[1] Saime Cigdem Yorulmaz. *Beyond photon pairs.* Casimir PhD series, Delft-Leiden, 2014.

[2] Wouter H. Peeters. *Two-photon interference.* Casimir PhD series, Delft-Leiden, 2010.

[3] Christopher C. Gerry and Peter L. Knight. *Introduction Quantum Optics.* University Press, Camebridge, 2005.

[4] Stephen M. Barnett and Paul M. Radmore. *Methods in Theoretical Quantum Optics.* Oxford University Press Inc., New York, 1997.

[5] M.M. Schipper. *The Campbell-Hausdorff theorem.* Bachelor thesis, University of Leiden, 2014.

[6] Anthony E. Siegman. *Lasers.* University Science Books, Mill Valley, 1986.

[7] Hugues de Riedmatten. *Two independent photon pairs versus four-photon entangled states in parametric down-conversion.* Journal of Modern Optics, vol. 51, no. 11, 1637–1649, 2004.